View metadata, citation and similar papers at core.ac.uk
brought to you by CORE
provided by Repository of the Academy's Library

Gold and silver catalysts for abatement of environmentally harmful materials: modelling the structure dependency
NNF 78837 project

Publications:

1. Iablokov V. Frey K., Geszti O., Kruse N.: High catalytic activity in CO oxidation over unsupported MnO_x nanocrystal, *Catalysis Letters, 134 (2010) 210-216*
2. Timea Benkó, Andrea Beck, Olga Geszti, Róbert Katona, Antal Tungler, Krisztina Frey, László Guczi, Zoltán Schay: Selective oxidation of glucose versus CO oxidation over supported gold catalysts**,** *Applied Catalysis A: General, 388, 31-36, 2010*
3. O. Hakkel, Z. Pászti, A. Berkó, K. Frey, L. Guczi: In situ sum frequency generation vibrational spectroscopy study of CO adsorption on Au surfaces promoted by Ar^+ sputtering and FeO_x additives, *Catalysis Today, 158 (1-2), 63-68, 2010*
4. A. Sárkány, Z. Schay, K. Frey, É. Széles, I. Sajó: Some features of acetylene hydrogenation on Au-iron oxide catalyst, *Applied Catalysis A: General, 380, 133-141, 2010*
5. A. Beck, G. Magesh, B. Kuppan, Z. Schay, O. Geszti, T. Benkó, R. P. Viswanath, P. Selvam, B. Viswanathan, L. Guczi: Specific role of polymorphs of supporting titania in catalytic CO oxidation on gold, *Catal. Today, 2011 (in press)*
6. Krisztina Frey, Gábor Pető, Katalin V. Josepovits and László Guczi: Gold catalysts for the abatement of environmentally harmful materials: modelling the structure dependency, *Vacuum, 2011 (in press)*
7. M. Veres, M. Koós, S. Tóth, K. Frey, G. Pető, P. Hargittai, L. Himics, A.V. Karmenyan, E. Perevedentseva: Nanocrystalline diamond supported gold catalyst for CO oxidation, *Diamond and Related Materials, 2011 (submitted)*
8. Zs. Baji, A. Szanyo, Gy. Molnár, A. Tóth, K. Frey, G. Pető: Formation of nanoparticles by ion beam irradiation of thin films, *Journal of Nanoscience and Nanotechnology, 2011 (in press)*
9. Pál Tétényi; Tamás Ollár; Tibor Szarvas: Sulfur exchange capacity and thiophene hydrodesulfurization activity of sulfided molybdena-alumina catalysts promoted by nickel, *Catalysis Today, 2011 (submitted)*
10. L. Guczi, A. Beck, Z. Pászti: Gold Catalysis: Effect of Particle Size on Reactivity towards Various Substrates, *Catalysis Today, 2011 (submitted)*
11. Krisztina Frey, Louis M Lubango, Mike S. Scurrell and László Guczi: Light alkanes aromatization to BTX over modified Zn-ZSM-5 catalysts. Characterization of the catalysts by hydrogen/deuterium isotope exchange, *Catalysis Communications, 2011 (under submission)*

Conferences:

1. T. Benkó, A. Beck, L. Guczi, A. Tungler, Z. Schay**:** Selective D-glucose oxidation over gold catalyst support effect, *COST Chemistry D36 3rd Workshop, Benahavis (Malaga, Spain), 2009 (poster)*
2. Frey Krisztina: Oxalátos lecsapatással készült nanoszerkezetű katalizátorminták (Ag/TiO_2, MnO_x) szerkezeti és katalitikus jellemzése, *Katalízis Munkabizottsági ülés, oral, 2010*
3. Krisztina Frey, Gábor Pető, Viacheslav Iablokov, Norbert Kruse and László Guczi: Gold and silver catalysts for abatement of environmentally harmful materials: modelling the structure dependency, *Indo-Hungarian Workshop on „Future Frontiers in Catalysis" NCCR, IIT Madras, (oral), 2010*

4. T. Benkó, A. Beck, L. Guczi, A. Tungler, Z. Schay: Selective D-glucose oxidation over gold catalyst support effect, *Budapesti Műszaki és Gazdaságtudományi Egyetem Vegyészmérnöki Kar Oláh György Doktori Iskolájának VII. Konferenciája, Budapest, 2010 (poster)*
5. A. Beck, Z. Schay, T. Benkó, G. Magesh, B. Kuppan, B. Viswanathan, L. Guczi: Effect of different titania polymorphs on catalytic activity of Au/TiO_2, *COST D36/003/06 Working Group Meeting, 21-22 May 2010, Sibiu, Romania (oral)*
6. L. Guczi, G. Magesh, A. Beck, Z. Schay, B. Kuppan, T. Benkó, B. Viswanathan: Anomalous behaviour of different allotropic forms of titania in Au/TiO_2 catalysts, *TOCAT6/APCAT5, July 18-23, 2010, Sapporo, Japan (oral)*
7. T. Benkó, A. Beck, O. Geszti, R. Katona, L. Guczi, A. Tungler, K. Frey, Z. Schay, Selective oxidation of glucose versus CO oxidation over supported gold catalysts, *TOCAT6/APCAT5, July 18-23, 2010, Sapporo, Japan (poster)*
8. Krisztina Frey, Gábor Pető, Ferenc Tanczikó and László Guczi: Gold and silver catalysts for abatement of environmentally harmful materials: modelling the structure dependency, JVC13 Conference, June 20–24, 2010 in Štrbské Pleso (oral)
9. T. Benkó, A. Beck, L. Guczi, A. Tungler, Z. Schay, K. Frey: Supported gold catalysts in selective oxidation of D-glucose**,** *International Symposium on Catalysis, Kraków, Poland, 29 August – 2 September, 2010 (poster)*
10. Krisztina Frey, Viacheslav Iablokov, Miklós Veres, István Sajó, Olga Geszti, Guczi László and Norbert Kruse: High catalytic activity in CO oxidation and PROX reactions over MnO_x nanocrystals, *10th Pannonian International Symposium on Catalysis, Kraków, Poland, 29 August – 2 September, 2010 (oral)*
11. M. Veres, M. Koós, S. Tóth, K. Frey, G. Pető, P. Hargittai, A.V. Karmenyan, E. Perevedentseva: Nanocrystalline diamond supported gold catalyst for CO oxidation**,** *21st European Conference on Diamond, Diamond- Like Materials, Carbon Nanotubes, and Nitrides, 5-9 September 2010, Budapest, Hungary (poster)*
12. Timea Benkó, Andrea Beck, Antal Tungler, László Guczi, Krisztina Frey, Zoltán Schay: Supported gold catalysts in selective glucose oxidation and CO oxidation, *6th EFCATS Summer School, „Catalysis & Surface Science for Renewables & Energy", 13-19 September, 2010 Izmir, Turkey (poster)*
13. Frey Krisztina: Research in the Institute of Isotopes, HAS, *Regional Training Course on Characterization of Nano-structures, Hacettepe University, Department of Chemistry in Ankara, Turkey, 8-12 November, 2010 (oral)*
14. Frey Krisztina: Nagy aktivitású MnO_x nanokristályok szerkezeti és katalitikus jellemzése, *Katalízis Munkabizottsági Ülés*, *Budapest 2010. december 10***.** *(oral)*
15. Krisztina Frey, Timea Benkó, Olga Geszti, László Guczi, Zoltán Schay: SiO2 supported Ag-Au alloy nanoparticles with high catalytic activity in selective oxidation of glucose, *COST Chemistry D36 4th Workshop, 18-20 May, 2011, Fuengirola, Spain (oral)*
16. Frey K., Benkó T., Geszti O., Schay Z. and Guczi L.: SiO_2 supported Ag-Au alloy nanoparticles with high catalytic activity in different reactions, *EuropaCatX, 28 August – 2 September, 2011 Glasgow, Scotland*
17. Frey K., Iablokov V., Sáfrán Gy., Osán J., Sajó I., Szukiewicz R., Chenakin S. and Kruse N.: High catalytic activity in CO oxidation over MnO_x nanocrystals, *EuropaCatX, 28 August – 2 September, 2011 Glasgow, Scotland*
18. Ollár Tamás, Szarvas Tibor, Tétényi Pál: Behaviour of catalyst sulfur in the hydrodesulfurization process, *EuropaCatX, 28 August – 2 September, 2011 Glasgow, Scotland*

SCIENTIFIC REPORT OF NNF 78837 PROJECT

Automotive exhaust gas contains significant amounts of NO_x, CO and hydrocarbons, which are all harmful to human health. Although the emission of these components can be drastically reduced by using a three-way catalyst, nitrous oxide, N_2O, is produced during the catalytic reaction, which has a strong greenhouse effect. Since catalysts produce undesired by-products like N_2O, not only the human-health effects, but also environmental aspects must be considered when implementing an automotive-exhaust emission control strategy. This is even more so in view of the increasing importance of lean burn engines where NO_x is to be reduced under net oxidizing conditions.

In addition to the CO oxidation, the selective oxidation of glucose was also studied, although it was not foreseen in the proposal. Many efforts were described in the literature to oxidize selectively the aldehyde group of D-glucose to produce gluconic acid. This latter is a high-value product for fine chemical industry. During the last two decades Pt- and Pd-based catalysts have been extensively studied in the oxidation of that multifunctional molecule. These had high activity but low selectivity. The best catalytic performance was achieved with Bi-promoted Pt-Pd catalyst supported on carbon, but the metal leaching and self–poisoning effects could not be avoided. It was found in our preliminary experiments that the catalysts prepared for CO oxidation are also effective in this reaction. These supported samples could also help to develop industrially relevant, Pd- Pt–free catalysts for this reaction.

The present project is aimed at developing a novel family of catalysts, based on gold and silver, to replace the more expensive Platinum and Rhodium metals. Such precious metals are the most promising replacements as active catalysts for automotive exhaust gas pollutants abatement and also for selective oxidation of glucose.

In this work we wanted to investigate and compare the various preparation techniques to produce a well-defined catalyst structure. For this purpose, gold and silver nanoparticles were evaporated in a well-controlled process onto SiO_2-covered Si(100) wafers using several new techniques. We created model catalysts having an interface between gold and different oxides such as TiO_2, FeO_x and CeO_2, in different morphology (fabricating of the layers or particles of the two components). This makes it possible to investigate the metal/support effect and to model the structure effect. The following categories of samples were prepared and studied:

1. ***Model samples***:

- *Fe/Au/SiO_2/Si(100) and Fe/Ag/SiO_2/Si(100)*: the samples were prepared by molecular beam epitaxy (MBE) technique, using the MECA-2000 MBE instrument of the KFKI Research Institute of Particle and Nuclear Physics. The Au or the Ag layer was deposited first to the substrate. To do so, the Au was evaporated from a graphite crucible using a high-temperature (HT) effusion cell. For the Ag, an Al_2O_3 crucible was applied for the evaporation, while the Fe was evaporated using an electron gun. Several samples were prepared, where the thicknesses of the Fe deposits were either 10 nm or 40 nm, whereas the Au or Ag underneath of Fe were 5nm or 20 nm. The SiO_2 on Si(100) substrate was 300 nm thick. After evaporation the samples were kept in air for oxidation of Fe layer. From the XPS results we concluded that the "as prepared" 10 nm Fe overlayer is continuous and fully covers the Au/SiO_2/Si(100) or Ag/SiO_2/Si(100) surface. It is composed of Fe_2O_3 (Fe^{3+}), FeO (Fe^{2+}), some metallic Fe and FeOOH. The X-ray Diffraction (XRD) measurements confirmed the presence of metallic Fe on the surface and the orientation of Au was (111). The FeO_x was not detected by XRD due to its amorphous structure. The AFM (Atomic Force Microscopy) of „as prepared" 10nmFeO_x/20nmAu/SiO_2/Si(100) showed very smooth surface with a RMS of 1.39 nm (Fig. 1a). After several catalytic tests on the surface particles with 30-50 nm height and 100-200 nm diameter were formed (RMS=23.9) (Fig. 1b). In Fig. 1c the catalytic activities of the tested samples in CO oxidation are presented. After 60 min treatment in 200 Torr H_2 at 573K

the samples were heated up to 803K in vacuum, then a mixture of 9 Torr CO + 18 Torr O_2 + 153 Torr He was introduced. The 10nm FeO_x/20nm Au/300nm SiO_2/Si(100) sample (Fig 1c/3) showed high activity in the CO oxidation reaction. The 300nm SiO_2/Si(100) (Fig 1c/1), 10nm FeO_x/300nmSiO_2/Si(100) (Fig 1c/2) and 20nm Au/300nm SiO_2/Si(100) (not shown) samples were much less active [3].

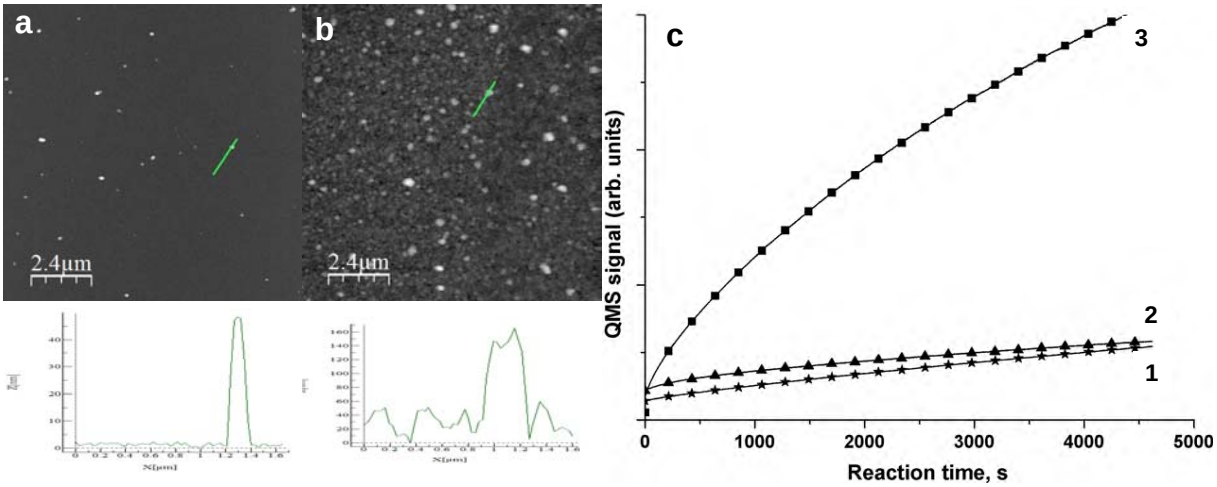

Fig. 1: AFM images of 10nm FeO_x/20nm Au/SiO_2/Si(100) before CO oxidation (a) and after several tests (b). CO_2 formation vs. reaction time for CO oxidation (c) over 300nm SiO_2/Si(100) (1), 10nm FeO_x/300nm SiO_2/Si(100) (2) and 10nm FeO_x/20nm Au/300nm SiO_2/Si(1 00)(3).

The stability of the samples was studied as well as the effects of different pre-treatments (reduction and calcination) on the catalytic activity in CO oxidation reaction. In Fig. 2. the catalytic activities of 10nm FeO_x/20nm Au/SiO_2/Si(100) sample are shown after different pre-treatment steps. Before a second catalytic test the sample was not pre-treated in order to investigate the stability in CO oxidation. The catalytic activity decreased in the second run which can be explained with a partial re-oxidation of FeO_x overlayer during the first reaction. The catalytic activity of the sample drastically decreased after calcination but after a reduction treatment it was more active than after the second catalytic test. We got the same results for all FeO_x-covered Ag or Au model samples. The effect of the subsequent pre-treatments was followed by XPS measurements. The reduction and calcination treatments were done in-situ with H_2 at 573 K and with air at 673 K for 1 hour, respectively. The 10 nm FeO_x layer reduced to metallic Fe during the reduction treatment in H_2 (Fig. 3a) and after calcination the Fe overlayer became again a mixed FeO_x. The Au 4f spectra (Fig. 3b.) demonstrate a very interesting effect. In "as prepared" and after calcination state there was no gold detected on the surface, but during the reduction pre-treatment the gold apparently moved up to the surface or close to the surface. Therefore the high catalytic activity after reduction pre-tretament can be explained with the effect of metallic iron over the Au layer which is different from the FeO_x overlayer prepared by PLD (pulsed laser deposition) method (published earlier).

The FeO_x/Ag/SiO_2/Si(100) samples were found to be more active in CO oxidation than the FeO_x/Au/SiO_2/Si(100) samples. The 5nm Ag/SiO_2/Si(100) had superior activity under these circumstances and the 20nm Ag/SiO_2/Si(100) was much more active than 20nm Au/SiO_2/Si(100). The 5 and 20nm Ag layer was covered with 10 and 40nm Fe layer by MBE, respectively. The catalytic activities of different samples are presented in Fig. 4. The following trend of CO oxidation activity was found: 40nm FeO_x/Ag/SiO_2/Si(100) >> 10nm FeO_x/Ag/SiO_2/Si(100)> 10nm FeO_x/SiO_2/Si(100) ≅ 40nm FeO_x/SiO_2/Si(100) in the case of 5nm Ag or 20nm Ag, respectively.

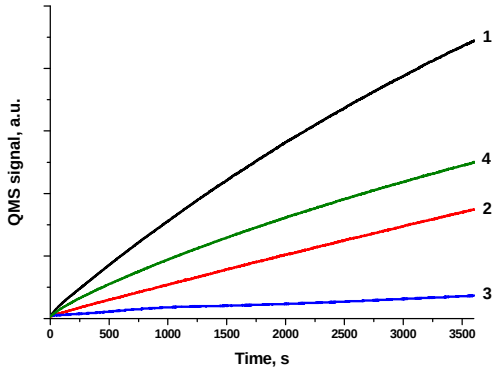

Fig. 2.: CO_2 formation vs. reaction time for CO oxidation over 10nm FeO_x/20nm $Au/SiO_2/Si(100)$ sample: 1. cycle after reduction (in 200 Torr H_2 at 573 K for 1h) (1), 2. cycle without pre-treatment (2), 3. cycle after calcination (in 200 Torr O_2 at 673K for 1 h) (3) and 4. cycle after reduction pre-treatments (4).

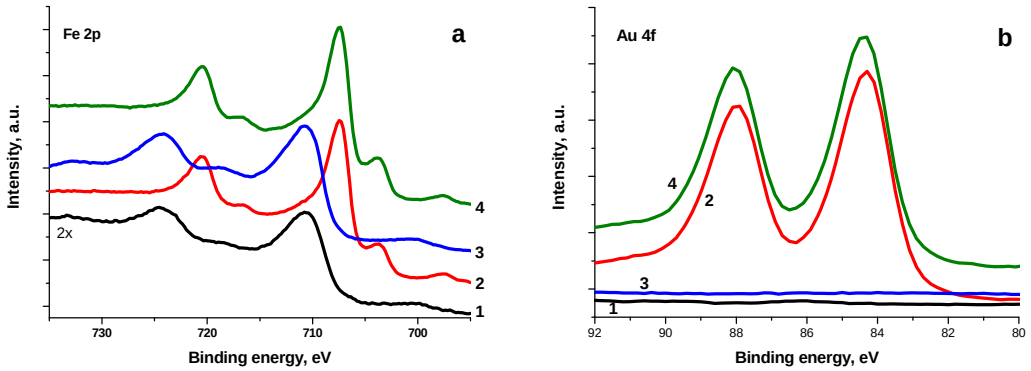

Fig. 3.: XPS Fe 2p (a) and Au 4f (b) spectra of 10nm FeO_x/20nm $Au/SiO_2/Si(100)$: "as prepared" state (1), after in situ reduction (in H_2 at 573 K for 1h) (2), after in situ calcination (in air at 673K for 1 h) (3) and after in situ reduction pre-treatments (4).

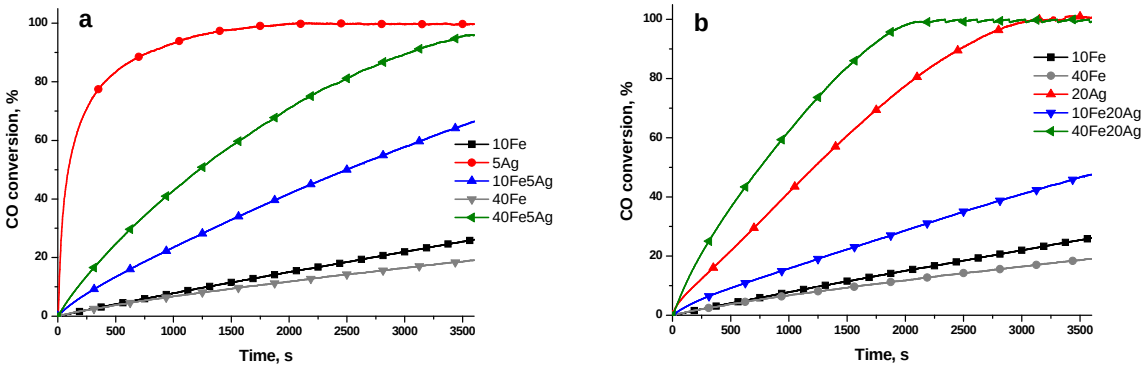

Fig. 4.: Conversion vs. reaction time for $Ag/SiO_2/Si(100)$ samples with 5nm (a) or 20nm (b) thickness of Ag and $FeO_x/Ag/SiO_2/Si(100)$ with 10nm or 40nm thickness of FeO_x overlayer.

- *Ag or $Au/SiO_2/Si(100)$:* These samples were also prepared by the MBE technique. Just like in the procedure described above, the Au layer was prepared using the HT effusion cell. For the Ag, however, an Al_2O_3 crucible was taken for the evaporation. These samples were

rotated during the deposition in order to obtain an even better layer homogeneity. The thickness of the Au layer was nm or 20 nm. The thickness of Ag deposit was 5, 10, 15 or 60 nm.

The surface structure of the evaporated Ag was studied by AFM (Fig. 5.).

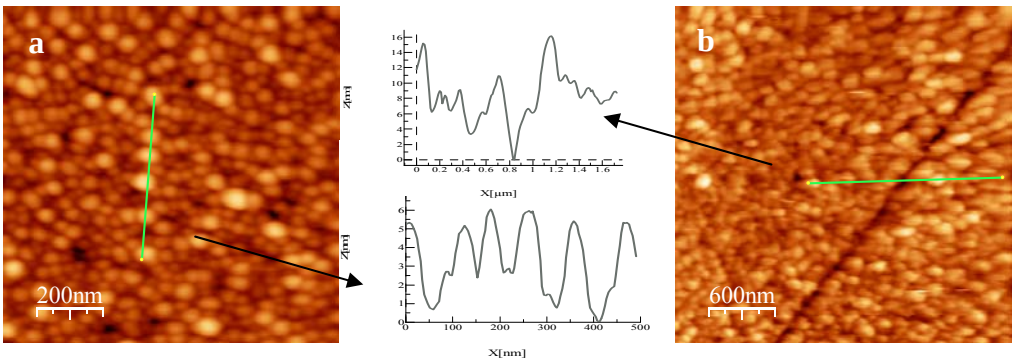

Fig. 5.: AFM images of 5nm Ag/SiO_2/Si(100) (a) and of 15nm Ag/SiO_2/Si(100) sample.

The AFM picture of 5nm Ag/SiO_2/Si(100) (Fig. 5a) showed Ag particles with 4-5 nm height and ca. 30-40 nm diameter. The shape of these elements is mostly hemispherical. The 15nm Ag layer is not smooth (Fig. 5b) and on the surface there are Ag particles with 2-8 nm height and 50-200 nm diameter. The presence of Ag particles on the surface can explain the higher catalytic activity in CO oxidation compared to the Au/SiO_2/Si(100) samples. The catalytic activity curves of Ag/SiO_2/Si(100) samples are presented above in Fig. 4. The 5nm Ag/SiO_2/Si(100) has a higher catalytic activity than that of 20nm Ag/SiO_2/Si(100) which result is similar to the Au/SiO_2/Si(100) samples (it was studied and published earlier).

The change in the electron structure of Ag was followed by XPS and UPS (KRATOS, ESCA) and also by synchrotron radiation excitation in MAX lab. The size dependence of the valence band and the atomic core level is characteristic for the nanoparticles as we already presented earlier on other different element besides Au. We measured energy distribution curve of photoelectrons (EDC's) excited from the valence band of Ag nanoparticles in the range of 20-140 eV of the excitation photon energy. At the low photon energy range (20-40 eV), the decrease of the photoelectrons excited from 4d states at low binding energy was observed. At the 140 eV photon energy the decrease of the photoelectrons excited from the full 4d states was found. On the other hand, the relative increase of photoelectrons excited from states near Fermi level was detected.

- *CeO_2/Au/SiO_2/Si(100):* In a cooperation with the Charles University of Prague we had an opportunity to prepare samples using a magnetron sputtering system. The deposition rate was at least 200 nm per hour. The 6 nm or 20 nm gold layers prepared by MBE were subsequently covered by CeO_2 using this sputtering technique. The thicknesses of CeO_2 layers were 10, 20, 30, 40 or 50 nm. We characterized the model samples by XRD, SEM, ellipsometry and XPS techniques. From the XRD results it was observed that the Au layer is always (111)-oriented and the ceria layer is CeO_2 which is in line with the XPS results. From the SEM pictures the evaporated CeO_2 overlayers appear to be very smooth and continuous. The thicknesses of ceria and gold layers were calculated from the SEM images and ellipsometry measurements.

The samples were tested in CO oxidation reaction using same conditions as it was described above. The samples were pre-treated in 200 Torr hydrogen at 573 K for 60 minutes before the catalytic test. The catalytic activities of the samples are presented in Fig. 6.

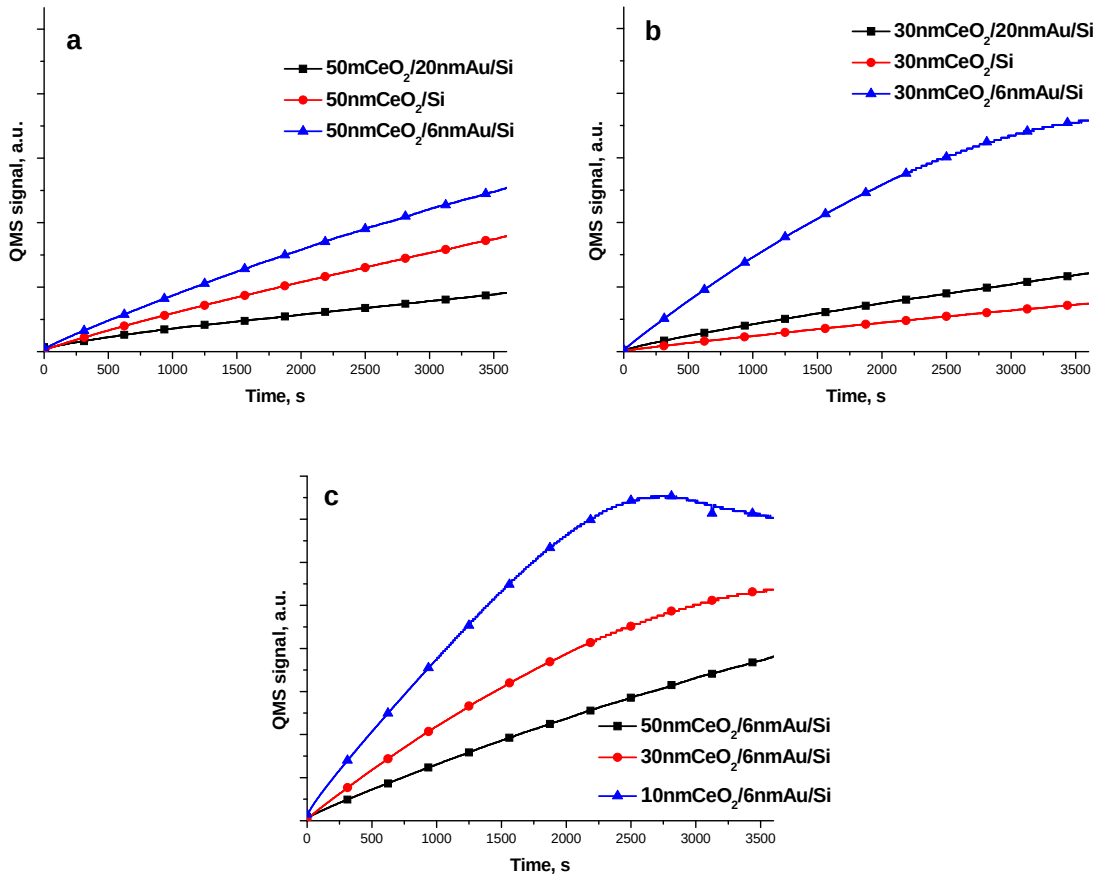

Fig. 6.: Activity vs. reaction time for CO oxidation over different CeO_2/Au/SiO_2/Si(100) samples.

The CeO_2/6nm Au/SiO_2/Si(100) had a higher catalytic activity in CO oxidation than CeO_2/20nm Au/SiO_2/Si(100) (Fig. 6 a and b). The activity increased with the decreasing of the CeO_2 thickness (Fig. 6c). The stability and the effect of the pre-treatment were studied on these systems. Before the 1st cycle the samples were reduced in 200 Torr hydrogen, before the 2nd cycle there was no treatment (to study the stability of the samples), before 3rd cycle the sample were calcined in 200 Torr O_2 at 673K for 60 minutes and finally before the 4th cycle a reduction treatment was applied. The samples had the highest catalytic activities in the first cycle, and there was not much difference between the 2nd, 3rd or 4th cycles. It was observed that the CeO_2 layer is much less sensitive for the treatments than the FeO_x layer. The change of the oxidation states during the different treatments were followed by XPS. In the "as prepared" state and after calcination the ceria layer contained Ce^{4+} while after reduction Ce^{3+} was also presented (Fig. 7.).

To compare preparation methods of sputtering and pulsed laser deposition, a 20 nm gold film was evaporated onto SiO_2/Si(100) wafer by electron beam evaporation. In the above case, CeO_x films were deposited sputtering, and with the present set of samples by PLD (pulsed laser deposition) method. Different thicknesses of Ce-oxide were created by 100, 300 and 500 pulses PLD method on the top of Si wafer covered with native SiO_2. The CeO_x overlayer made by 100 pulses was measured to be 15 nm thick, as calculated from XRD measurements. The Ce 3d XPS spectra of all of the CeO_x/Au/SiO_2/Si(100) model samples are composed of Ce^{3+} and Ce^{4+}. The composition of the deposited CeO_x overlayer depends on the thickness and whether there is gold underneath or not. These structural differences can explain our catalytic results of the CeO_x/Au/SiO_2/Si(100) model system (Fig. 8.). The initial activity of

100CeO_x/Au/SiO_2/Si(100) was significantly lower than that of 100CeO_2/SiO_2/Si(100) where higher amount of Ce^{3+} was in the layer. 600CeO_x/Au/SiO_2/Si(100) was significantly more active than 600CeO_2/SiO_2/Si(100) which contains more Ce^{4+} formation in the oxide layer. The promoting or inhibiting effect of gold depends on the ratio of Ce^{3+}/Ce^{4+} in the CeO_x overlayer. Where the structure of CeO_x did not show large changes, the catalytic activity is quite similar with gold or without gold [6].

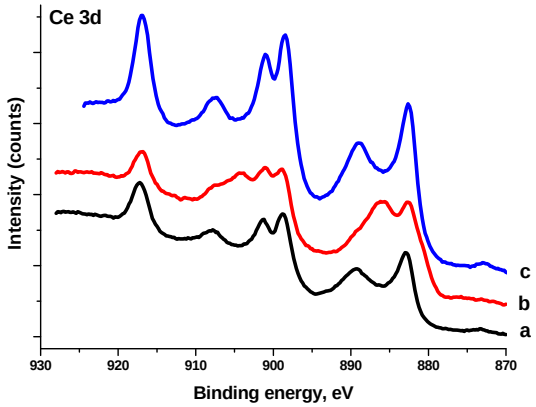

Fig. 7.: XPS Ce 3d spectra of the (a) "as prepared", (b) reduced and (c) calcined 10 nm CeO_2/20nm Au/SiO_2/Si(100) sample.

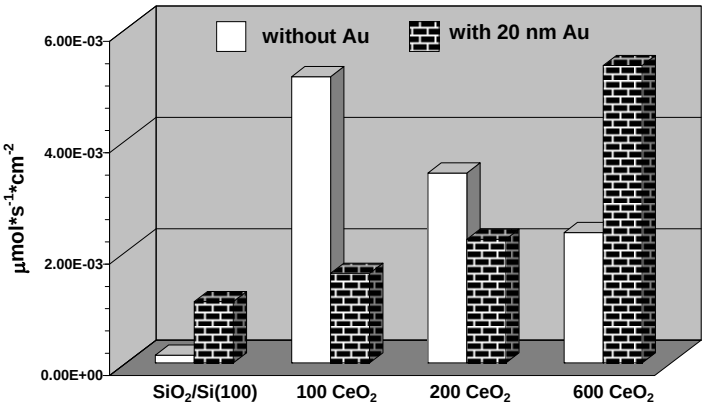

Fig. 8: Initial reaction rates of CeO_x/Au/SiO_2/Si(100) and CeO_x/SiO_2/Si(100) samples with different thickness of CeO_x overlayer

- *Fe/FeAu/SiO_2/Si(100)*: these samples were prepared by MBE using co-evaporation of Fe and Au. The thickness of the Fe deposit was 10 nm, and $Fe_{50}Au_{50}$ was 30 nm. The samples were characterized by XPS and tested in CO oxidation. The Fe in the FeAu layer is in metallic state. Fe/$Fe_{50}Au_{50}$/SiO_2/Si(100) was more active than $Fe_{50}Au_{50}$/SiO_2/Si(100) in CO oxidation reaction. The stability and effect of treatments were studied also on these systems. The following trend was observed: 4^{th} cycle > 1^{st} cycle > 2^{nd} cycle > 3^{rd} cycle on the 10nm FeO_x/30nm $Au_{50}Fe_{50}$/SiO_2/Si(100). When Fe was oxidized the catalytic activity of the samples decreased dramatically. However, with a repeated reduction the samples became active again or even more active than in the first cycle. The explanation of these findings is still under investigation.

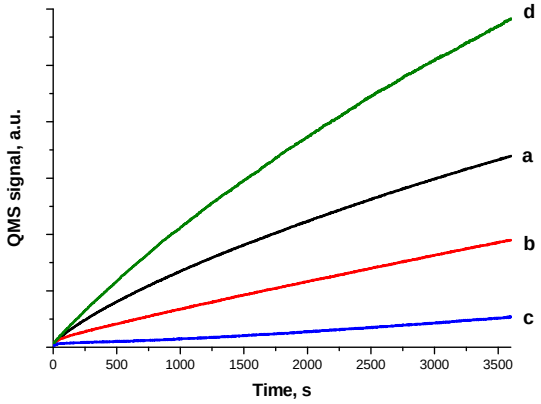

Fig. 9.: CO_2 formation vs. reaction time for CO oxidation over 10 nm FeO_x/30nm $Au_{50}Fe_{50}/SiO_2/Si(100)$ sample: (a) 1st cycle (after reduction), (b) 2nd cycle (no treatment), (c) 3rd cycle (after calcination) and (d) 4th cycle (after second reduction).

- *Fe/AgAu/SiO_2/Si(100)*: the samples were prepared by MBE using co-evaporation of Ag and Au. The thickness of the Fe deposit was 10 nm or 40 nm, and the AgAu alloy was 30 nm ($Ag_{20}Au_{80}$, $Ag_{50}Au_{50}$, $Ag_{80}Au_{20}$).

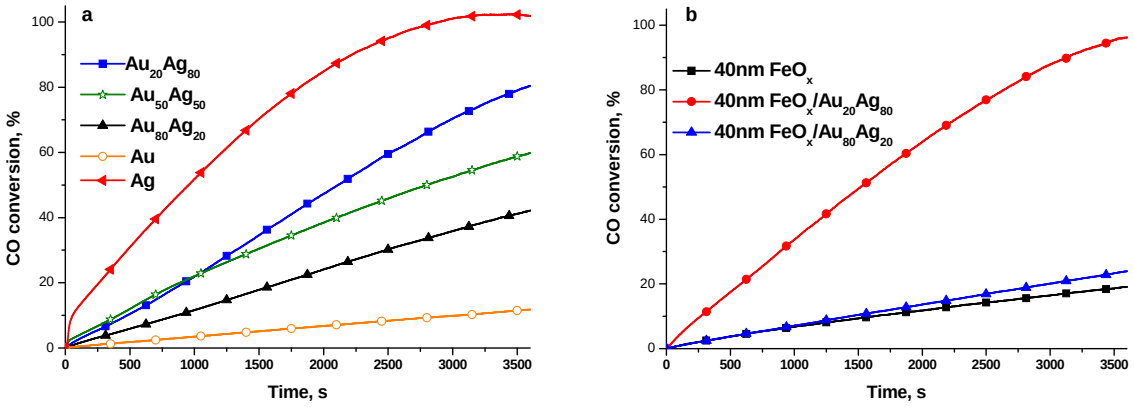

Fig. 10.: CO conversion vs. time over 30 nm $Au_yAg_z/SiO_2/Si(100)$ (a) and 40nm $FeO_x/Au_yAg_z/SiO_2/Si(100)$ (b) samples.

The samples were tested in CO oxidation reaction. The catalytic activity depends on the Au-Ag ratio; the silver-rich catalysts are significantly more active than the gold-rich ones with or without FeO_x cover (Fig 10. a and b). The increasing catalytic activity is nearly linear with the Au/Ag ratio, which means there is no synergism effect between the gold and silver particles in CO oxidation reaction.

- *Au/diamond/SiO_2/Si(100)*: Nanocrystalline diamond crystallites (100 nm average grain size) were immobilized on Si substrate using laser acceleration technique. Gold was deposited on top of this system by sputtering. Depending on the sputtering time Au nanoparticles, fragmented film and continuous layer were formed on diamond crystallites. The morphology and the structure of the system were investigated using SEM, XPS and Raman methods. The Au nanoparticles/diamond/SiO_2/Si(100) presented the highest catalytic activity in CO oxidation in this sample category [7].
- *TiO_2/Au/SiO_2/Si(100):* Thin gold films (8 or 60 nm) were deposited by electron gun evaporation in a VT 460 evaporator at UHV onto Si(100) wafer covered with native SiO_2 of nanometer thickness range. The TiO_2 layer was deposited on the top of the gold film by PLD (pulsed laser deposition) using 100 pulses of a Nd laser source (it was prepared and partly

published earlier). The sample surfaces were studied by TOF-SIMS. On the surface of TiO_2 covered $Au/SiO_2/Si(100)$, in both the Au nanoparticles case and the 60 nm-thick Au film case, no gold and no Si was detected by SIMS, and the titanium oxide layer seemed to be continuous. The thickness of 100 pulses of TiO_2 was calculated from SIMS spectra and it was found to be 14 nm. From the Ti2p XPS spectra the $TiO_2/Au/SiO_2/Si(100)$ is composed of TiO_2 (Ti^{4+}). By XRD no anatase signal was visible in the as-prepared state; it only became visible after CO oxidation when a simultaneous increase in Au particle size is observable, accompanied by restructuring indicated by the reversed intensity ratio between Au(200) and Au(111). The structural changes can play a major role in the decreased activity of a repeated catalytic test. The initial activity of $TiO_2/Au/SiO_2/Si(100)$ was significantly lower than that of $TiO_2/SiO_2/Si(100)$, while $Au/SiO_2/Si(100)$ was the least active. The inhibiting effect of gold on the catalytic activity of the TiO_2 overlayer was discussed in terms of electronic interactions at the Au/TiO_2 interface. TiO_2 films of different thickness were also successfully prepared by PLD method (100, 300 and 500 pulses). Catalytic reaction rate measurements (see Fig. 11.) of different thickness of $TiO_2/SiO_2/Si(100)$ showed no difference. The inhibiting effect of gold was highest when the TiO_2 overlayers were prepared by 300 laser pulses. If the layer thickness is larger than it would be created by 500 pulses, there is no significant difference in the reaction rates. It can be concluded that inhibition of TiO_2 activity by Au ranges occurs over relatively short distances less than 70 nm (calculation from SIMS measurements where 100 pulses was 14 nm) [6].

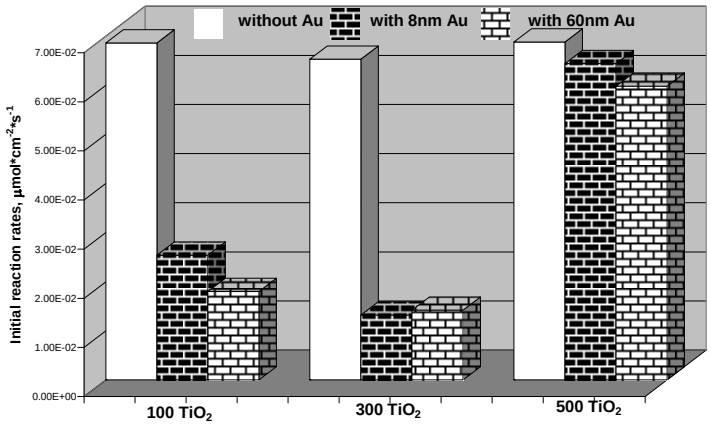

Fig. 11.: Initial reaction rates of $TiO_2/Au/SiO_2/Si(100)$ and $TiO_2/SiO_2/Si(100)$ samples with different thickness of gold layer or TiO_2 overlayer

2. High surface area supported samples:

- *Au/FeO_x*: Au-iron oxide catalysts containing 3.0, 4.5, 5.6 wt% Au prepared by deposition-precipitation (DP) with urea, adsorption of Au sol (SA) and co-precipitation (CP) of $HAuCl_4$ and $Fe(NO_3)_3$, respectively. The latter method produced Au particles supported on amorphous 2-line ferrihydrite ($Fe_5HO_8{\cdot}4H_2O$). Au/iron oxide catalyst precursors (Au/α-Fe_2O_3 and Au/2-line ferrihydrite) were characterized by BET, TGA, TPR and XRD, and the Au particle size by TEM measurements. The TPR measurements confirm the ease of transformation of 2-line ferrihydrite to magnetite (Fe_3O_4) and that the formation of magnetite from α-Fe_2O_3 depends strongly on the size of the gold and the supporting oxide particles. Particle size effect of gold was investigated in semi-hydrogenation of acetylene. Reduction of α-Fe_2O_3 (hematite) into Fe_3O_4 is a sensitive function of both Fe_2O_3 and Au particle size. Au/FeO_x catalysts are highly selective in semi-hydrogenation of acetylene and the ethane formation selectivity is less than 1% in the 323–473K temperature range. The hydrogenation is accompanied with oligomer formation, the C4+ selectivity is typically 2–

4%. Our results on Au/FeO_x provide some data on the particle size sensitivity of acetylene semi-hydrogenation. The observed particle size sensitivity emphasizes the role of low-coordination sites in activation of hydrogen molecules. The TPO results confirm that the Au surface under working conditions is covered by hydrocarbons/deposits. The ageing of the catalysts (time on stream experiments) appears to be affected by the particle size. XRD measurements confirmed formation of homogeneous Au–Fe particles (30–40 at% Fe) and Fe^0 supported on magnetite. Formation of Fe0 and AuFe particles significantly increased the hydrogenation activity but decreased the semi-hydrogenation selectivity [4].

- *Au/TiO_2:* In cooperation with National Centre for Catalysis Research, IIT, Madras different type TiO_2 samples were used as support. Brookite was intended to be prepared by two preparation methods from $TiCl_4$ and $TiCl_3$ producing BRT4 and BRT3, respectively, Degussa P25 was applied as reference. Gold was deposited using the sol method by adsorption of citrate/tannic acid reduced and stabilised Au sol on titania. The adsorption was assisted by preadsorption of PDDA polycation on titania increasing the attraction with Au nanoparticles of negative surface charge. To remove the organic residues the washed and dried samples were calcined before the CO oxidation catalytic tests. For comparison, Au/BRT4 and Au/P25 was prepared by deposition precipitation (DP). According to XRD measurements BRT4 contained 100% brookite, while BRT3 was composed of 55% anatase and 45% brookite. Degussa P25 TiO_2 contains 85% anatase and 15% rutile. The specific surface area of BRT4, BRT3 and P25 was 114, 197 and 55 m^2/g, respectively. By comparison the CO oxidation activities and taking into account the particle sizes of Au and TiO_2 it could be concluded the intrinsic activity of Au-anatase is larger than that of Au-brookite [5].
- Preparation of *supported gold catalysts*: SiO_2, CeO_2 and TiO_2 supported gold catalysts were prepared by sol adsorption method. The Au colloids were prepared from $HAuCl_4$ solution reduced and stabilized with Na-citrate and tannic acid (TC) or reduced by $NaBH_4$ and using polyvinylalcohol (PVA) as stabilizer. The average Au particle size was 6-7 nm (TC sol) and 2-3 nm (PVA sol). After Au sol adsorption on SiO_2, CeO_2 and TiO_2 supports the samples were calcined. After calcination the Au loading was ~ 2 wt% in the catalysts. The particle size distribution was determined by Transmission Electron Microscopy (TEM) and the metal loading was determined by Inductively Coupled Plasma Mass Spectrometry (ICP-MS). After calcination the Au particle size increased to 5-7 nm (PVA sol) and 7-13 nm (TC sol), respectively. The samples were tested in CO oxidation and selective glucose oxidation reactions. Inverse correlation was found between the activities in glucose oxidation and CO oxidation (Fig. 12.) suggesting that the mechanisms are different which is explained by geometrical and support effects. The results showed that the effect of the support is more significant than the small gold particle size [2].

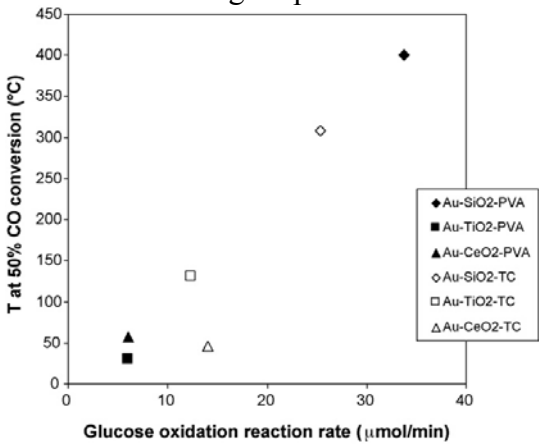

Fig. 3: Comparison of activities in CO oxidation and glucose oxidation.

- Preparation of *supported silver and Ag-Au alloy catalysts*: Silica, ceria and titania supported silver catalysts were prepared by sol adsorption method: preparation of Ag colloid reducing $AgNO_3$ with sodium borohydrate in the presence of polyvinylalcohol (PVA) as stabilizer followed by adsorption of *Ag-sol* on
  (i) SiO_2 (Davisil) at pH 1 adjusted by HCl (*Ag-SiO_2*)
  (ii) CeO_2 (*Ag-CeO_2*) by addition of poly (diallyldimethylammonium chloride) (PDDA). This polycation adsorbing on the support surface increased the attraction between the support and the colloid Au particles stabilised by negatively charged PVA shell
  (iii) TiO_2 (P25) (*Ag-TiO_2*) by addition of poly (diallyldimethylammonium chloride) (PDDA)

The samples were filtered, washed and dried at 333 K overnight.

Ag-Au alloy catalysts supported on SiO_2, TiO_2 and CeO_2 were prepared by colloidal deposition. Ag-Au alloy nanoparticles with different Ag/Au ratio were prepared in colloidal phase by reducing first $AgNO_3$ with sodium borohydride in the presence of PVA followed by elimination of the excess $NaBH_4$. In the next step $HAuCl_4$ was added into the silver sol and repeatedly reduced by $NaBH_4$, in the presence of polyvinylalkohol (PVA) as stabilizer and followed by adsorption of Ag-Au-PVA on the support (SiO_2, TiO_2, CeO_2). The color of the silver sol was yellow which turned brown after some minutes of mixing and turned purple during Ag-Au alloy nanoparticles formation. In the samples the nominal metal loading was 2 wt% with different Au-Ag ratio: Ag/SiO_2, $10Ag90Au/SiO_2$, $20Ag80Au/SiO_2$, $33Ag67Au/SiO_2$, $50Ag50Au/SiO_2$, $80Ag20Au/SiO_2$, Au/SiO_2, the numbers in the sample notation refer to the relative atomic percentages of the metals. Before the catalytic test the samples were calcined at 400°C in air (50ml/min) for the removal of organic residues. To confirm the Ag-Au alloy structure UV-Vis and HRTEM measurements of the sols were taken. TEM measurements were used to calculate the particle size of the sols.

Only one peak was detected by UV-Vis spectrophotometer in the case of Ag-Au alloy sol and the position of that peak was in the visible region between the peak of the monometallic Ag sol and Au sol, whereas the in the case of a mixture of Ag sol and Au sol two peaks were detected at the original positions (Fig. 13.).

HRTEM measurements showed no phase contrast in the particles, they seemed to have homogeneous alloy structures. It was not possible to use the lattice parameters of Au and Ag crystals for differentiation of Au and Ag by HRTEM, because Ag and Au have the same crystal structure and the lattice constants are very similar.

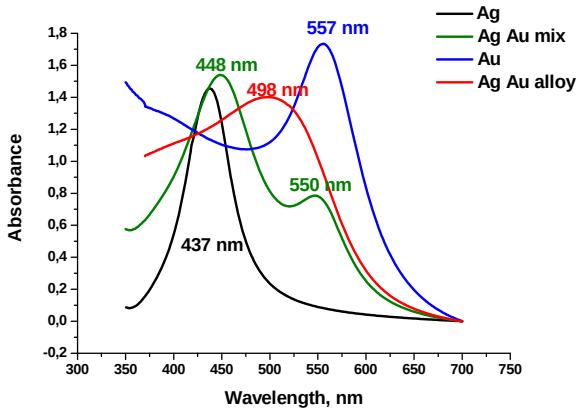

Fig. 13.: UV-VIS spectra of Ag, Au AgAu alloy and AgAu mixture sols.

The AgAu nanoparticles were supported on SiO_2. The average AgAu alloy particle size was 3.3 ± 0.9 nm in 20Ag80Au/SiO_2 sample. The AgAu nanoparticles were more stable against than the monometallic Ag nanoparticles..

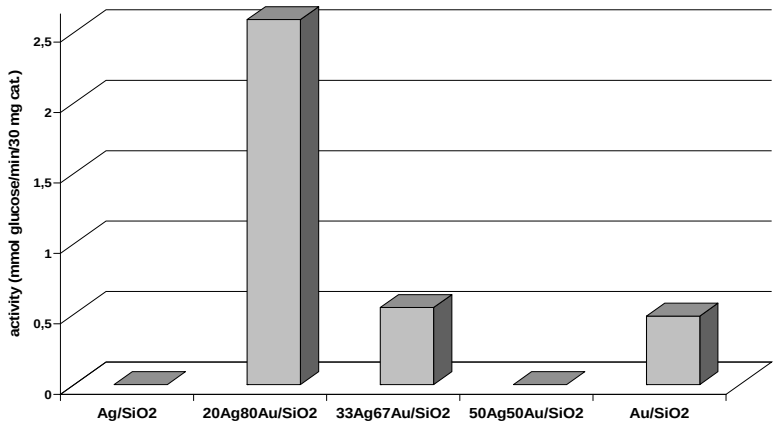

Fig. 14.: Glucose oxidation activities over AgAu/SiO_2 samples

The samples were tested in glucose oxidation. The analysis of the reaction products was performed by HPLC on a JASCO instrument equipped with a Jasco UV 2075 and an ERC7515A RI detector. A Hamilton HC-75H+ form cation exchange column was used with aqueous succinic acid as eluent. With this system it is possible to measure the concentration of glucose in the presence of gluconic acid. Under these conditions selectivity was always 100%. In gold catalyzed total oxidations as e.g. CO oxidation the smaller gold particle size and the reducible oxide supports favour the activity. In our previous work in glucose oxidation the SiO_2 supported larger size gold was more active. Synergetic activity increase was detected in the case of 20Ag80Au/SiO_2 and 33Ag67Au/SiO_2 alloy catalysts. The 20Ag80Au/SiO_2 sample was 5 times more active than the reference Au/SiO_2. The activity decreased drastically in the case of 50% or more Ag content in the alloy nanoparticles. (Fig. 14.) The possible explanation could be that small amounts of Ag helped the activation of oxygen while at high Ag content the activity decreased by the strong adsorption of oxygen.

The sol derived Au and/or Ag containing catalysts supported on silica, titania and ceria were tested in temperature programmed CO oxidation and NO+CO reaction. Before catalytic reaction the samples were calcined in 20%O_2/N_2 at 673K for 1h for removal of organic residues. The activity difference between Ag and Au is small in case of SiO_2 supported systems (Fig. 15 and 16). On TiO_2 the large Ag particles (Fig. 17) are more active than the 13 nm Au ones (Fig. 15), but less active than the 5-6 nm gold particles. The monometallic Au/CeO_2 samples prepared by adsorption of either $NaBH_4$ reduced and PVA stabilized (denoted by "_PVA") or tannic acid-sodium citrate reduced and stabilized (denoted by "_TC") sols (Fig.15) were significantly more active in CO oxidation than the monometallic Ag/CeO_2 (Fig.18) partly because the particle size of Au is smaller than Ag. (Note that the contact time in case of Ag-catalysts was 2 times higher.) The Au-Ag bimetallic effect was studied at different Au/Ag molar ratio. The Au67Ag33/SiO_2 sample gave higher activity than the monometallic analogous. This could be the consequence of the smaller size of the bimetallic particles; however the other, less active bimetallic samples contains also smaller particles, so the Au/Ag composition must play a role, too. Nevertheless, the same AuAg sol derived Au67Ag33/TiO_2 and Au67Ag33/CeO_2 did not show similarly enhanced activity compared to the other TiO_2 and CeO_2 supported catalysts, respectively.

The adsorption of sols on titania or ceria were not fully successful and coagulation may have taken place that could be the reason of the formation of very large particles in the calcined samples. The AuAg/TiO_2 samples were less active than the monometallic ones. On

the contrary, the ceria supported sample of Au/Ag=20:10 presented higher activity than Ag/CeO_2 and also $Au67Ag33/CeO_2$ was more active than the silica supported analogous.

The stability of the catalytic activity and the effect of reducing pre-treatment, TPR up to 793K, are demonstrated in case of Ag/TiO_2 catalyst on Fig. 19. The catalyst activity was reproducible in the repeated catalytic runs and no significant change was observed after TPR. Many other catalysts deactivated somewhat after the first temperature programmed reaction, but the next runs were more stable, that is why the second heating up cycles was compared.

Concerning the NO reduction by CO neither the silica, nor the titania supported samples were active, while CeO_2 supported systems converted about 40-60% of NO at 673K (Ag/CeO_2 was the most active) which is less than that was measured on MnO_x derived form oxalate and Au/MnO_x (Fig. 20). The NO decomposition activity order of the two ceria supported bimetallic samples is reverse compared to their CO oxidation activity order.

Summarizing, the monometallic silver catalysts prepared by the sol method described above did not exceed the CO oxidation activity of the analogous monometallic Au catalysts. The AuAg bimetallic particles formed by $NaBH_4$ reduction and PVA stabilization were significantly smaller than the corresponding silver particles. On silica support the high dispersion could have been retained, but on TiO_2 and CeO_2 strong sintering was detected, which originated likely by the coalescence of the metal nanoparticles in the adsorption step. On the bimetallic effect we cannot draw solid conclusion, yet, because we could not prepare mono and bimetallic systems with similar size. Improvement of the adsorption of bimetallic sol may provide much higher activity samples on titania and especially on ceria.

According to our results the MnO_x can be a good component of the catalyst for the basic reactions for automotive pollution control. We will continue the investigation of manganese oxides in our next project (NNF 85631).

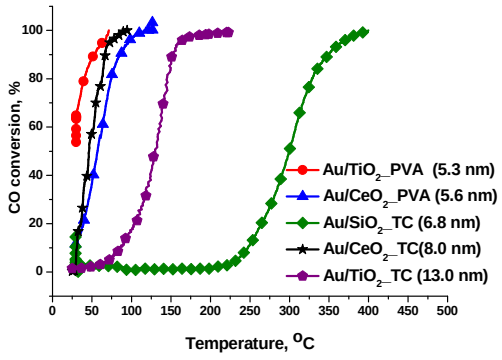

Fig. 15.:
CO oxidation activity of gold on different supports after calcination (60 mg catalyst, 0.5% CO, 9% O_2 in He, 55 ml/min, 4°C/min, the values in parenthesis are the mean diameter of Au particles in the calcined samples).

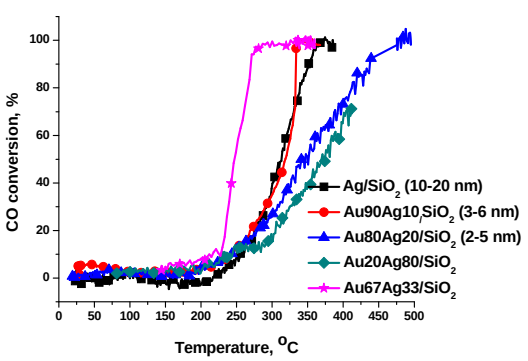

Fig. 16.: CO oxidation activity of SiO_2 supported Ag and bimetallic AuAg after calcination (30 mg catalyst, 0.5% CO, 10% O_2 in He, 13.8 ml/min, 5°C/min, the values in parenthesis are the mean diameter of metal particles in the calcined samples).

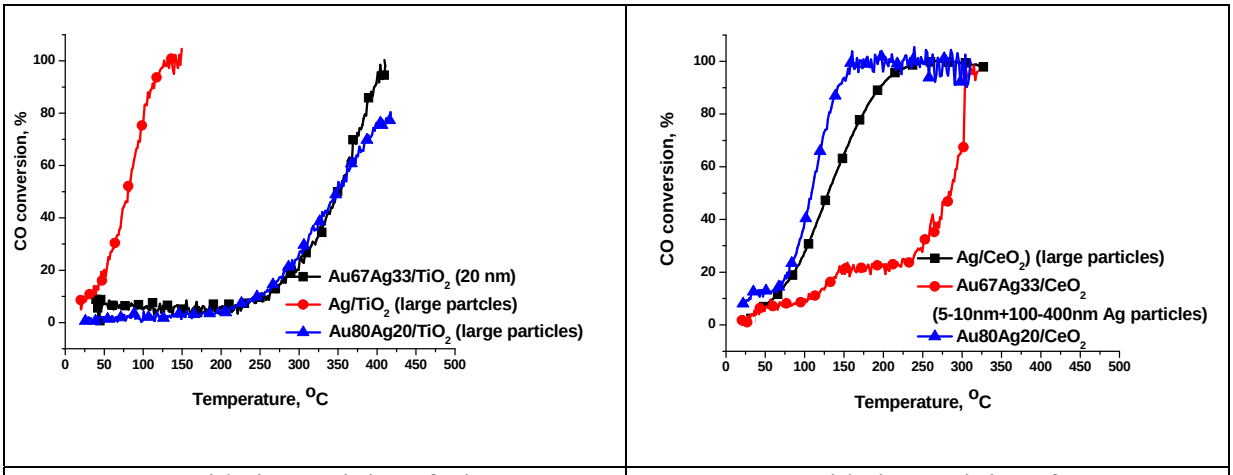

Fig. 17.: CO oxidation activity of TiO_2 supported Ag and bimetallic AuAg after calcination (30 mg catalyst, 0.5% CO, 10% O_2 in He, 13.8 ml/min, 5°C/min, the values in parenthesis are the mean diameter of metal particles in the calcined samples).

Fig. 18.: CO oxidation activity of CeO_2 supported Ag and bimetallic AuAg after calcination (30 mg catalyst, 0.5% CO, 10% O_2 in He, 13.8 ml/min, 5°C/min, the values in parenthesis are the mean diameter of metal particles in the calcined samples).

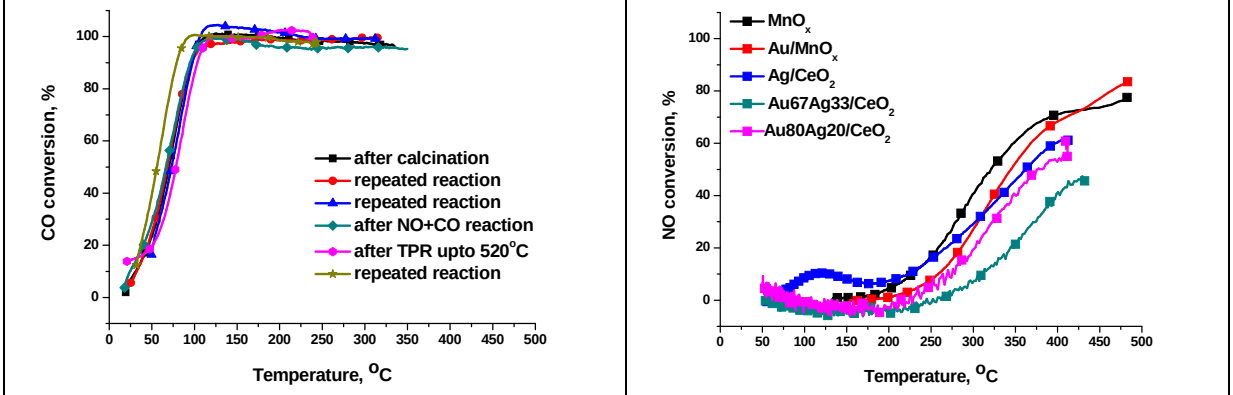

Fig. 19.: CO oxidation activity on Ag/TiO_2 catalysts after different consecutive treatments (60 mg catalyst, 0.8% CO, 20% O_2 in He, 12.5 ml/min, 5°C/min).

Fig. 20.: NO conversion on CeO_2 supported Ag and bimetallic AuAg and MnO_x and MnO_x supported Au after calcination (30 mg catalyst, 0.67% CO, 0.67%NO in He-Ar, 15 ml/min, 10°C/min).

- *Ag/MnO_x:* In a cooperation with the Université Libre de Bruxelles the catalysts were prepared by oxalate co-precipitation in water using $AgNO_3$ and $Mn(NO_3)_2$*$4H_2O$ as precursors at room temperature while stirring vigorously and adjusting the pH value between 5 and 6 using ammonia. The precipitation was gradual with an induction period of 3–5 min. After 40 min the precipitate was filtered, washed in water and dried overnight at 343 K in an oven. The as prepared Mn-oxalate was subsequently transformed into manganese oxide using temperature programmed oxidation (TPO). Ag loadings in the catalysts were 0, 2, 4, 7, and 10 % (w/w)*:* After TPO activation the gas flow was switched to a CO + O_2 mixture (2% of each) in Ar as carrier gas at atmospheric pressure with a flow rate of 50 mL/min for the CO oxidation studies. Comparatively the most active catalyst is the pure MnO_x. The Ag content did not play a considerable role in the catalytic activity of Ag/MnO_x. We continued our studies only on the pure MnO_x. The temperature of 50% CO conversion was T_{50} = 260 K. The pure manganese oxide is nonstoichiometric MnO_x (x = 1.61…1.67). The activity gradually decreased with time-on-stream of the reactants but could be easily recovered by heating at 633 K in the presence of oxygen. CO oxidation over MnO_x in the absence of oxygen proved

to be possible with reduced rates and demonstrated a Mars—van Krevelen—type mechanism to be in operation. A TEM structural analysis showed the MnO_x phase to form microrods with large aspect ratio which broke up into nanocrystalline manganese oxide (MnO_x) particles with diameters below 3 nm and a BET specific surface area of 525 m^2/g. Annealing at 798 K rather than 633 K produced well crystalline Mn_2O_3 which showed lower CO oxidation activity, i.e. 100% CO conversion at 335 K (Fig. 15.) [1].

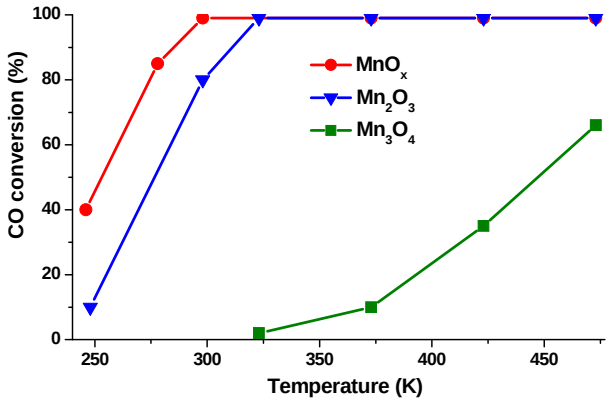

Fig. 15.: Conversion vs. temperature for MnO_x, Mn_2O_3 and Mn_3O_4

- *Au/MnO_x*: Extra high surface area MnO_x possesing high CO oxidation catalytic activity was prepared by calcination of Mn-oxalate produced from $Mn(NO_3)_2$*$4H_2O$ and oxalic acid in the previous year of the project. Recently the modification of this type of Mn-oxide by gold is aimed and its effect in the catalytic CO oxidation and preferencial CO oxidation in large excess of H_2 is studied. Au/MnO_x was prepared by two different methods. Au nanoparticles were deposited on a newly produced MnO_x by deposition precipitation using urea and by adsorption of Au sol containing nanoparticles of 2-3 nm in diameter. MnO_x and DP prepared Au/MnO_x have been tested catalytically, the sol derived sample is under investigation at present. Mn_3O_4 phase and Au particles with wide size distribution (5-300 nm in diameter) were recognised in the DP prepared Au/MnO_x after a series of oxidative and reductive pre-treatments followed by catalytic tests. We expect smaller Au sizes and narrower size distribution in case of sol derived samples. The Mn-oxide did not show the high surface area and the special needle-like morphology as expected, but it consisted of rather spherical small particles, however still performed significant catalytic activity which was further increased in case of DP formed Au/MnO_x ($T_{50\%}$ was lowered by 333-343 K). The calcination pre-treatment slightly decreased the activity of the as prepared MnO_x sample, additional reductive treatment caused further small deactivation. In case of Au/MnO_x the as prepared form were as active as the as prepared MnO_x, but the sample were activated during the reaction and in a repeated temperature programmed catalytic run much larger activity was observed wich was stable after calcination and only slightly decreased after reduction. Also in PROX the gold containing system was more active and the maximum CO conversion was higher (35%) than that of MnO_x (23%), but still very low. The reduction treatment decreased the PROX performance in both catalysts.

Summary

The model system investigations could widen our knowledge on the interaction of gold and so called active oxides (FeO_x, TiO_2, CeO_2) in catalytic CO oxidation. The earlier observed and described indirect effects of gold (layers or nanoparticles) on the catalytic activity of FeO_x overlayer have been supported with further evidences. Additionally, formation of metallic iron was detected, which had strong effect on the catalytic activity of

the system. The operation of the special interaction of inverse oxides/metal interface was revealed for other oxide/metal compositions as well, like FeO_x, TiO_2, CeO_2, on Ag, Au or bimetallic AuAg and AuFe. Several parameters (layer thicknesses, stability, pre-treatments etc.) affecting this phenomenon were investigated.

The AuAg interaction was studied also on high surface area supported systems. Alloyed AuAg particles were prepared, stabilized on different supports (FeO_x, TiO_2, CeO_2) and tested in different catalytic reactions (CO oxidation, NO_x reduction, selective glucose oxidation). Only in the case of selective glucose oxidation could be observed a strong AuAg synergism on SiO_2 support. Although in CO oxidation and NO_x reduction processes we found higher activity bimetallic sample as compared to the monometallic reference, the origin of increased activity (as e.g. particle size effect or special cooperation of two metals) could not be clearly elucidated. It needs further investigations and production of more controlled samples.

Among studied support materials high surface area and nonstoichiometric MnO_x derived from oxalate precursor was found to be a very promising catalyst component in these environmentally important reactions.

We would like to publish of the presented results in journals with high impact.